

A Water-Explicit Lattice Model of Heat-, Cold-, and Pressure-Induced Protein Unfolding

Bryan A. Patel,* Pablo G. Debenedetti,* Frank H. Stillinger,[†] and Peter J. Rossky[‡]

*Department of Chemical Engineering, [†]Department of Chemistry, Princeton University, Princeton, New Jersey; and [‡]Department of Chemistry and Biochemistry, Institute for Theoretical Chemistry, University of Texas at Austin, Austin, Texas

ABSTRACT We investigate the effect of temperature and pressure on polypeptide conformational stability using a two-dimensional square lattice model in which water is represented explicitly. The model captures many aspects of water thermodynamics, including the existence of density anomalies, and we consider here the simplest representation of a protein: a hydrophobic homopolymer. We show that an explicit treatment of hydrophobic hydration is sufficient to produce cold, pressure, and thermal denaturation. We investigate the effects of the enthalpic and entropic components of the water-protein interactions on the overall folding phase diagram, and show that even a schematic model such as the one we consider yields reasonable values for the temperature and pressure ranges within which highly compact homopolymer configurations are thermodynamically stable.

INTRODUCTION

Globular proteins remain in their functional native state in a limited range of temperatures and pressures, unfolding into denatured states at both high and low temperature and high pressure (1,2). Fig. 1 shows the characteristic parabolic shape of a protein phase diagram, for the specific case of Staphylococcal nuclease (3). The stability of the native state is the result of several contributions, including van der Waals, electrostatic, and hydrogen-bonding interactions, as well as configurational entropy (4). Walter Kauzmann first suggested that the hydrophobic effect plays a central role in protein stability on the basis of several observations (5). First, proteins tend to sequester the majority of their hydrophobic residues in the core of the molecule, avoiding exposure to water (6). Second, natural water-soluble proteins are unable to fold into their native states in nonpolar solvents (7). Finally, the free energy of transfer of a hydrophobic solute from its pure phase into water shows the same qualitative temperature dependence as the protein unfolding free energy. The liquid-hydrocarbon model of the protein core suggests that the temperature-dependent behavior of the enthalpy and entropy of unfolding is due largely to hydrophobic hydration phenomena (8).

The relevance of this simple picture to high-pressure protein stability is less certain. Kauzmann pointed out inconsistencies between the volume effects associated with protein unfolding and hydrocarbon transfer, thereby questioning whether the liquid-hydrocarbon picture can account for pressure denaturation. The volume change of hydrocarbon transfer is negative at low pressure and generally positive at high pressure, while the volume change of protein unfolding is positive at low pressure and negative at high pressure (9).

Calculations from an information theory model of hydrophobic interactions have reconciled these pictures by, in effect, inverting the liquid-hydrocarbon model for pressure effects; pressure denaturation is viewed as the penetration of the protein cavities by water molecules, more akin to the transfer of a water molecule into a pure hydrophobic phase (10,11).

Alternatively, recent theoretical work on the hydration of hydrophobic solutes of different sizes is also of relevance to hydrophobic homopolymer collapse (12–15). The hydration of large hydrophobic solutes is accompanied by density depletion at their interface with water, which can then resemble the interface between vapor and liquid water (12). Correspondingly, water density fluctuations at the interface would give rise to bubble formation, and bubbles of a critical size would span intermolecular distances and induce the collapse of large hydrophobic polymers (13). From this viewpoint, the stability of this collapsed state is reduced as the solvent moves away from vapor-liquid coexistence at low temperature and high pressure, giving rise to cold and pressure denaturation (12,14). This framework is consistent with the approach adopted here, in that the complexity of real proteins is reduced to an exclusive focus on the thermodynamics of hydrophobicity for the interpretation of the phase diagram of protein folding. A recent molecular dynamics simulation of a hydrophobic polymer in water has manifested the existence of a dewetted polymer-water interface in extended polymer conformations (15). The polymer also exhibited signatures of both warm and cold denaturation, with compact states remaining marginally stable only within an intermediate range of temperature, while extended configurations predominate at high and low temperatures.

Atomically detailed simulations of proteins have provided substantial insight into the mechanisms of protein denaturation and the formation of native-state structure. The choices of force field and whether to model the solvent implicitly or explicitly dictate the types of physical situations that these

Submitted March 8, 2007, and accepted for publication July 23, 2007.

Address reprint requests to Bryan A. Patel, Tel.: 609-258-5413; E-mail: patel@princeton.edu.

Editor: Jose Onuchic.

© 2007 by the Biophysical Society
0006-3495/07/12/4116/12 \$2.00

doi: 10.1529/biophysj.107.108530

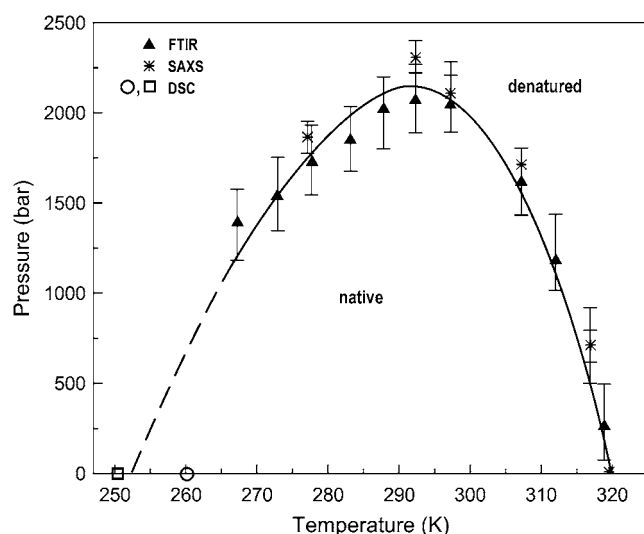


FIGURE 1 Phase diagram for Staphylococcal nuclease from Fourier transform infra-red (FTIR) spectroscopy, small angle x-ray scattering (SAXS) and differential scanning calorimetry (DSC) experiments. Adapted with permission from Ravindra and Winter (3).

simulations can tackle. Explicit-solvent molecular dynamics simulations are commonly used to study protein dynamics and hydration for small protein fragments of <40 residues. These studies have provided insight into protein folding pathways and intermediates for several different peptides and proteins, such as the villin headpiece (16,17), a β -hairpin (18), and BBA5 (19). Other studies have examined the role of water in hydrophobic collapse of the protein core and protein-water hydrogen bonding for larger proteins like the BphC enzyme (20) and ribonuclease A (21). High-pressure, explicit-solvent simulations utilizing water insertions into the protein interior have investigated the effect of water penetration into the hydrophobic core on pressure denaturation (22).

Modeling the solvent implicitly drastically reduces simulation complexity, allowing larger proteins to be simulated for longer times. These simulations are used to explore the folding dynamics of proteins (23–25) and the temperature dependence of protein folding (26,27). Implicit solvent approximations are often used in protein structure prediction, where faster computation is necessary and folding dynamics are less important (28,29).

In contrast to the wealth of existing simulations to study short-time dynamics, few detailed simulations have been done to study protein stability over a wide range of temperatures and pressures, a limitation resulting from the long times required to simulate large-scale conformational changes. One example of such a study is a replica exchange molecular dynamics simulation of a small peptide in TIP3P water that demonstrated both pressure and thermal denaturation, but also showed that pressure did not disrupt the studied α -helical structures (30,31).

The reduced description of interactions used in lattice models of proteins offer the opportunity to examine protein

thermodynamics without incurring the large computational expense of atomically detailed simulations. The HP model (32) is a lattice heteropolymer model with hydrophobic (H) and polar (P) monomers. It implicitly incorporates the hydrophobic effect through an attraction between hydrophobic monomers on the protein chain. This approach was used to study the designability and uniqueness of protein native states and to explore how sequence affects the folded structure (32,33). While a broad thermal denaturation transition does occur in the HP model, it does not manifest cold unfolding. Inherently, the model's ground state is also the protein's native state, which precludes the existence of a denatured state which is more stable than the native state at lower temperatures. An extension of the HP model (34–37) to include water explicitly (the HPW model) uses the Muller-Lee-Graziano water model (38,39) to describe the solvent degrees of freedom. The Muller-Lee-Graziano model uses a bimodal description of water, distinguishing between bulk and solvation shell waters in their energy and entropy. From exact enumeration of the configurations of short heteropolymers, Caldarelli and co-workers showed that both a warm and a cold denaturation transition are manifest in the HPW model (34).

Pressure effects have been less commonly treated in theoretical models. A mean-field model for heteropolymer collapse by Dill (40,41) was recently extended by Cheung and co-workers (42) to include pressure-induced weakening of the hydrophobic association of protein monomers. The model exhibits cold-, pressure-, and heat-unfolding but, because it invokes the mean-field approximation, it can only examine the effect of average sequence hydrophobicity on protein thermodynamics. Another model dealing with pressure effects was developed by Marques and co-workers (43). Placing an all-hydrophobic homopolymer and explicit water on a compressible two-dimensional square lattice, they observed cold, thermal, and pressure denaturation. However, their Hamiltonian coupled the compactness of the protein to the bulk water structure, linking a local property of the protein to an average bulk property of water. This feature of the Hamiltonian favors compact protein conformations at conditions where bulk water is highly hydrogen-bonded, in effect forcing the correct outcome a priori, rather than obtaining folding as a result of microscopic interactions. Furthermore, the model predicts that cold-unfolding occurs only at high pressure, a fact not supported by experiments (3,44).

Here we revise the model of Marques et al., and present a different lattice model of an all-hydrophobic protein in water. We distinguish between bulk and interfacial hydrogen bonding, incorporating ideas from Frank's iceberg model (45). From this simple treatment of protein-water interactions, we can investigate how hydrophobic solvation affects the stability of proteins. A physically meaningful treatment of hydrophobic interactions allows us to reproduce many of the experimentally observed features of protein conformational stability in the pressure-temperature plane, including cold denaturation at ambient pressure.

The outline of this article is as follows. We begin with a description of the microscopic model and discuss the flat histogram simulation techniques used to compute the model's density of states. We then examine the shape of the resulting protein phase diagrams and discuss the driving forces behind each of the denaturation transitions. Finally, we present the main conclusions, as well as possible extensions to the model, some of which we are currently investigating. The Appendices contain derivations of biased trial moves used in the simulations and analytical approximations used to interpret the results as well as illustrative results for the volumetric properties of small model hydrophobic solutes.

MODEL DESCRIPTION

Each site on a two-dimensional square lattice is occupied either by a water molecule or a protein monomer. The water molecules have four hydrogen-bonding arms, each associated with a neighboring lattice site. The orientation of a bonding arm on water molecule i associated with adjacent site j is described by the variable σ_{ij} . Each bonding arm can adopt q orientations, thus σ_{ij} can take on values between 1 and q . The orientations of bonding arms on the same water molecule are uncorrelated with each other. A hydrogen bond forms between two neighboring water molecules $\langle i, j \rangle$ when their bonding arms are properly oriented, satisfying the condition $\sigma_{ij} = \sigma_{ji}$ in the original version of the model (46), or a modified condition (to be described below) in this work. To account for the lower local density associated with the formation of hydrogen bonds, we treat the lattice as compressible, and the total volume expands uniformly by an amount Δv upon formation of a hydrogen bond. The Hamiltonian for the hydrogen-bonding interaction in the original water model (46,47) is

$$\mathcal{H}_W = -J \sum_{\langle i, j \rangle} \delta_{\sigma_{ij}, \sigma_{ji}} = -J N_{HB}, \quad (1)$$

where J is the strength of a hydrogen bond and the Kronecker delta $\delta_{\sigma_{ij}, \sigma_{ji}} = 1$ when $\sigma_{ij} = \sigma_{ji}$, and is zero otherwise. N_{HB} is the number of hydrogen bonds in the system. The hydrogen-bonding interaction originates from a lattice model of water used to investigate this substance's thermodynamic behavior, especially at supercooled conditions (46,47). The original model allowed for empty lattice sites unoccupied by either protein or water, and displays many of the distinguishing anomalies of water, including the isobaric density maximum (46), and the increase upon isobaric cooling of the magnitude of the isothermal compressibility, isobaric heat capacity, and thermal expansion coefficient (47). The current model (without empty lattice sites), while displaying anomalous behavior such as negative thermal expansion, does not capture all of these anomalies. In this work, as in the original model (46,47), we consider each of the bonding arms belonging to the same water molecule to be independent. This simplification was subsequently removed in a more

realistic model (48). Here we show that even the highly idealized water model with independent bonding arms gives rise to realistic folding behavior.

The protein is modeled as a self-avoiding walk with covalently attached monomers occupying nearest-neighbor sites on the lattice. The protein is a homopolymer and each monomer is nonpolar. The protein has no self-interaction aside from excluded volume effects. The nonpolar protein's only interaction with water is through its indirect effect on water-water hydrogen-bonding.

We redefine the hydrogen-bonding interaction of the pure water model by differentiating water molecules into two classes: bulk and interfacial. Frank and Evans identified the tendency of water molecules to form ordered "icelike" cages around nonpolar solutes (45). These interfacial water molecules avoid orientations in which their hydrogen-bonding arms point toward the hydrophobe and remain in low entropy configurations in the first solvation shell. However, in these restricted configurations the interfacial waters form stronger hydrogen bonds than observed in bulk (49). While a bimodal description of hydrogen bonding was also used in the HPW model, as already noted, that water model does not reproduce water's unusual thermodynamics nor does it treat pressure effects (34–37).

To adapt these principles to our model, we must first recast the orientational criteria for hydrogen bonding to generalize the model. Hydrogen bonding is said to exist when two nearest-neighbor water molecules have their bonding arms oriented such that they are within some tolerance λ , or $|\sigma_{ij} - \sigma_{ji}| \leq \lambda$. In the context of this new hydrogen-bonding criterion, a value of $\lambda = 0$ is equivalent to the original water model's condition of $\sigma_{ij} = \sigma_{ji}$. The range of acceptable orientation pairs differs between bulk water (λ_b) and interfacial water (λ_h). A pair of hydrogen-bonding water molecules is designated as interfacial when either member of the pair is adjacent to one or more protein monomers. A smaller range of hydrogen-bonding orientations for interfacial water molecules ($\lambda_h < \lambda_b$) is the origin in the model of the lower entropy of the interfacial hydrogen bonds in hydrophobic hydration. The tolerances λ_b and λ_h directly affect the fraction of orientation pairs suitable for bonding. The total number of possible orientation pairs is q^2 for a pair of bonding arms on adjacent water molecules. If one of the bonding arms has any orientation σ_{ij} out of q possible orientations, then its partner must have an orientation from $\sigma_{ij} - \lambda_h$ to $\sigma_{ij} + \lambda_h$ to satisfy the interfacial hydrogen-bonding criteria. Thus, there are $(2\lambda_h + 1)q$ possible interfacial bonding pair orientations out of q^2 total orientation pairs. Because $\lambda_h < \lambda_b$, a smaller fraction of orientation pairs will satisfy the bonding criteria interfacially ($(2\lambda_h + 1)/q$), than in the bulk ($(2\lambda_b + 1)/q$).

Along with the entropic cost of interfacial hydrogen bonds, there is an enthalpic bonus. Since those hydrogen bonds formed in reduced orientational entropy configurations around hydrophobic solutes less frequently sample the more distorted and weaker bonding structures present in bulk (49,50), they

are given an additional enthalpic contribution (J_H) on top of the base hydrogen-bond strength J . Thus, the complete Hamiltonian of our model is

$$\mathcal{H} = -JN_{HB} - J_H N_{XHB}, \quad (2)$$

where N_{XHB} is the number of interfacial hydrogen bonds. The total volume is calculated as

$$V = V_0 + N_{HB}\Delta v. \quad (3)$$

The system volume without hydrogen-bonding is V_0 , and $V_0 = v_0 N_{sites}$, where N_{sites} is the number of lattice sites and v_0 is the volume per lattice site.

Our model is related to that of Marques et al. (43), using the same representation of a protein in water as a hydrophobic homopolymer on a two-dimensional square lattice. However, we use a different Hamiltonian for the protein-water interactions, incorporating the entropic and enthalpic characteristics of water hydrogen bonding on a molecular level into a two-tiered framework. In contrast, as modeled by Marques et al. (43), the protein has a repulsive interaction with the solvent given by

$$\mathcal{H}_p = J_r \frac{N_{HB}}{N_w} (N_{c,max} - N_c). \quad (4)$$

N_c is the number of intramolecular protein-protein nearest neighbor contacts, $N_{c,max}$ is the maximum number of such contacts, and N_w is the number of water molecules in the system. The parameter $J_r > 0$ is the strength of the repulsive interaction between the protein and water. Marques and co-workers propose this repulsion as a way to represent the tendency of an apolar macromolecule to adopt compact conformations in the presence of water's low-density hydrogen bonded network. They hypothesized that the inability of water to form a low-density structure at high pressures causes pressure denaturation by weakening this effective repulsion between water and the hydrophobic molecule. To incorporate this effect, the energy penalty term in Eq. 4 becomes significant either when the protein is not maximally compact ($N_c < N_{c,max}$) or when the bulk water has formed a low-density hydrogen-bond network ($N_{HB} > N_w$). The inclusion of the total number of hydrogen bonds in this term links the single-protein energetics to the bulk water behavior. It is not surprising, then, that the system shows unfolding at high pressures since at those conditions the energy penalty vanishes as the hydrogen-bonding structure in the system disappears.

METHODS

We used a modified version of the Wang-Landau method to estimate the density of states, Ω (51). In the conventional Wang-Landau approach, the simulation performs a random walk in energy (U) with probability proportional to the reciprocal of the density of states $1/\Omega(U)$. The random walk is performed within the range of attainable energies in the model. The density of states is not known a priori, but is determined on-the-fly during the simulation. The simulation is initialized at a random configuration with the density-of-states estimator set at $\Omega(U) = 1$ for all energy levels. Trial

moves from an old configuration (o) to a new configuration (n) at energy levels U_o and U_n , respectively, are accepted with probability

$$P_{acc}(o \rightarrow n) = \min \left[1, \frac{\Omega(U_o)}{\Omega(U_n)} \right]. \quad (5)$$

Each time a state with energy U is visited in the simulation, the corresponding density of states estimate is updated by multiplying the existing value by a modification factor f , i.e.: $\Omega(U) \rightarrow \Omega(U)f$. An initial value for the modification factor of $f_0 = e^1 \approx 2.71828$ is often used to allow the system to sample all possible energy levels efficiently. Throughout the simulation a histogram counting the frequency of visits to each energy level $h(U)$ is also updated, i.e.: $h(U) \rightarrow h(U) + 1$. The random walk proceeds until $h(U)$ becomes sufficiently flat to ensure relatively even sampling of all energy levels. At infinite time, the random walk should converge to be 100% flat, when $h(U)$ has the same value for each energy U . However, for practical purposes, we allow the simulation to continue until $h(U)$ at each energy level is greater than some percentage of the average value $\langle h(U) \rangle$. When this condition is satisfied, the modification factor is reduced to $f_{new} = \sqrt{f_{old}}$, so as to refine the precision of the density of states estimation process. The energy histogram $h(U)$ is reset to zero and a new iteration started. The process continues until the histogram is again sufficiently flat and the modification factor is reduced accordingly. This procedure is repeated until f approaches unity to within some designated tolerance.

In our simulations, we employ a slightly different strategy for determining the density of states that is adapted specifically to our model (43). Instead of a random walk in energy space, we perform a random walk in the two variables in our system Hamiltonian: N_{HB} and N_{XHB} . Any state specified by these variables corresponds to a specific system energy and volume given by Eqs. 2 and 3. The outcome of these simulations is the density of states, $\Omega(N_{HB}, N_{XHB})$, which can then be translated to $\Omega(U, V)$. The advantage of performing a random walk in N_{HB} and N_{XHB} , as opposed to U and V , is that the parameters J , J_H , and Δv need not be assigned values during the simulation. This allows us to gather the system thermodynamics for any parameter set from a single simulation.

Here we consider the histogram of visited states to be flat if every bin of $h(N_{HB}, N_{XHB})$ is at least 80% of the average histogram $\langle h(N_{HB}, N_{XHB}) \rangle$. The simulation ends when the modification factor is $< \exp(10^{-8})$. To improve sampling of rare protein configurations we also used several biased protein trial moves in addition to conventional translational and orientational trial moves. An explanation and derivation of the acceptance criteria for these trial moves is given in Appendix A.

Due to the large number of system states sampled even for a relatively small protein ($\sim 85,000$ for 20 monomers), the density of states was subdivided into smaller overlapping regions for expediency. Even with a small subset of phase space to sample, the system states around and including the protein native state required that the simulation be run in parallel on multiple processors. The processors independently performed random walks in the same subset of phase space and periodically communicated their estimates for Ω and h with each other, simultaneously testing whether the criteria for histogram flatness had been satisfied. The complete simulation of a 20-monomer protein required nearly 6000 CPU hours. The simulation of proteins up to 50 monomers is possible with a recently developed method which decouples the protein and water contributions to the density of states. This technique will be explained in detail in a forthcoming publication.

Extracting protein properties from the simulation data requires converting the density of states into more useful metrics. Since the simulation involves fluctuations in both internal energy and volume, it is natural to reweight the density of states to represent the isobaric-isothermal ensemble. Given a pressure P and temperature T , the probability of a state, i , specified by N_{HB} and N_{XHB} , is

$$p_i(P, T) = \frac{\Omega(N_{HB}, N_{XHB}) e^{-\beta U(N_{HB}, N_{XHB}) - \beta P V(N_{HB})}}{\Delta(P, T)}, \quad (6)$$

where $\beta = 1/k_B T$ and Δ is the isobaric-isothermal partition function. We define the protein native state as the set of system states where the protein is

fully compact, when it has formed the maximum number of nearest-neighbor protein-protein contacts. Summing the probabilities of these compact states gives the probability that the protein is folded as

$$p_f(P, T) = \sum_{\text{compact states}} p_{N_{HB}, N_{XHB}}(P, T). \quad (7)$$

The change in free energy upon unfolding, ΔG , can then be calculated from the folding probability by using the equilibrium relation from the two-state model of protein folding

$$\Delta G(P, T) = G_{\text{unfolded}} - G_{\text{folded}} = RT \ln \left[\frac{1 - p_f(P, T)}{p_f(P, T)} \right]. \quad (8)$$

The transition between the folded and unfolded states occurs when $\Delta G(P, T) = 0$ or, equivalently, when $p_f(P, T) = 0.5$.

RESULTS AND DISCUSSION

Fig. 2 shows the phase diagram of a 17-mer protein, with contours showing constant probabilities of occupying the folded state. The model protein exhibits heat-, cold-, and pressure-unfolding and the dome of stable temperatures and pressures has the same qualitative shape as observed experimentally. The folded protein is stabilized by minimizing the exposed surface area of hydrophobic monomers, thereby limiting the number of interfacial water molecules forced to pay an entropic cost for hydrogen-bonding around the protein. This corresponds to the maximally compact conformation shown in Fig. 3 *a*. Upon increasing temperature, the protein gradually unfolds and exposes more hydrophobic monomers to the solvent. The thermal energy is sufficient to overcome the entropic cost of forming additional interfacial hydrogen bonds around the exposed monomers. The thermally denatured protein is an ensemble of conformations,

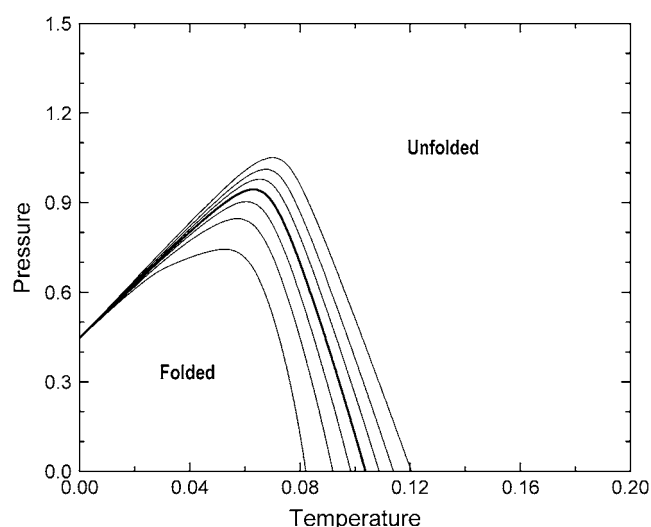


FIGURE 2 The phase diagram of a 17-mer homopolymer protein for $J_H/J = 0.2$, $\Delta v/v_0 = 0.348$, $\lambda_h = 0$, $\lambda_b = 1$, and $q = 30$. The inner line demarcates the region within which the probability of observing the folded state is 87.5% or greater. The other lines similarly demarcate the regions within which the folded probabilities are >75%, 62.5%, 50% (bold), 37.5%, 25%, and 12.5% (outermost).

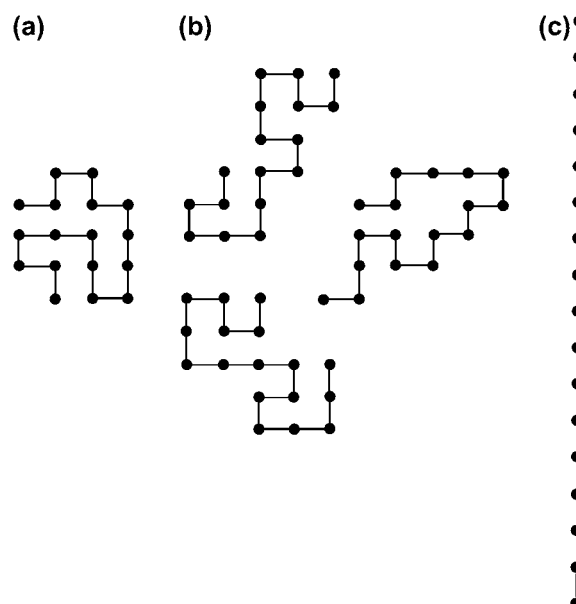


FIGURE 3 Representative conformations for a 17-mer model protein in the (a) native state, (b) thermally denatured ensemble of states, and (c) high-pressure cold-unfolded state.

with several examples shown in Fig. 3 *b*. At lower temperatures and high pressures the enthalpic benefit of additional interfacial hydrogen bonds drives the protein to unfold into a fully extended state, shown in Fig. 3 *c*. This configuration maximizes the number of water-protein contacts and allows for water to form the maximum number of interfacial hydrogen bonds.

The importance of the entropic penalty and the enthalpic bonus in cold and pressure denaturation is illustrated in Figs. 4 and 5. When $\lambda_b = 0$, there is no entropic penalty (since $\lambda_b = \lambda_h = 0$ in this case) and one sees that the protein is not susceptible to cold denaturation. The entropic penalty was applied by increasing λ_b while holding $\lambda_h = 0$. Increasing the entropic penalty increases the slope of the cold denaturation transition line as well as the maximum pressure at which the protein is stable at any nonzero temperature. This effect will be explained quantitatively below. Fig. 5 shows that there is no cold unfolding without the enthalpic bonus. Increasing the enthalpic bonus increases the stability of the cold-denatured state at the expense of the folded state. At $J_H/J = 0.3$, the protein shows cold denaturation even at zero pressure, while for $J_H/J > 0.3$ the protein no longer folds at positive pressures. The effect of changing J_H demonstrates that the formation of stronger hydrogen bonds between the water molecules close to the protein is also a required driving force for cold-unfolding in this model.

An analytical expression derived in Appendix B yields further insight into the mechanism of cold denaturation in this model. It is shown there that the transition pressure between the native and unfolded states at zero temperature can be calculated analytically, and is given by

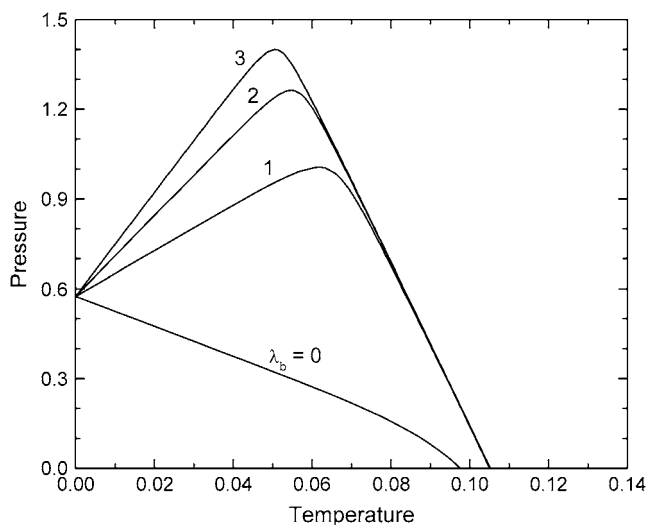


FIGURE 4 Contours of 50% folded probability for a 20-mer protein for varying values of the entropic penalty for forming interfacial hydrogen bonds. Simulations were performed with $\lambda_h = 0$ and changing λ_b . To retain the same bulk water thermodynamics, the total number of water orientations q increases such that the fraction of bonding configurations for a pair of bonding arms on adjacent molecules (i.e.: $(2\lambda_b + 1)q/q^2 = (2\lambda_b + 1)/q$) is kept constant, at 0.1. The other model parameters remain constant at $J_H/J = 0.2$ and $\Delta v/v_0 = 0.348$.

$$P_t \Big|_{T_t=0} = \frac{J}{\Delta v} + \frac{J_H}{\Delta v} \left(\frac{\Delta N_{\text{XHB}}}{\Delta N_{\text{HB}}} \right). \quad (9)$$

ΔN_{XHB} and ΔN_{HB} are the differences in the number of interfacial and total hydrogen bonds between the native and unfolded states, respectively. When the protein unfolds in this model, the bulk water must break a few hydrogen bonds to accommodate the extended protein structure, and $\Delta N_{\text{HB}} < 0$. The opening of the protein, however, allows more in-

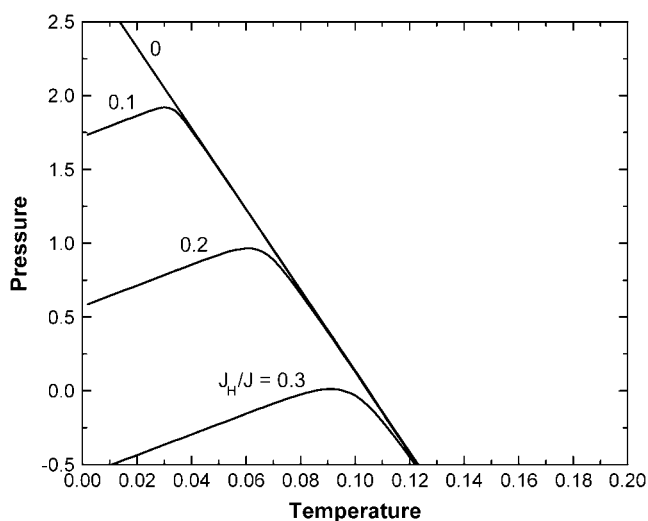


FIGURE 5 Contours of 50% folded probability for a 20-mer protein for varying values of the enthalpic bonus for interfacial hydrogen bonds J_H/J . The other model parameters are $\Delta v/v_0 = 0.348$, $\lambda_b = 1$, $\lambda_h = 0$, and $q = 30$.

terfacial hydrogen bonds to be formed, and $\Delta N_{\text{XHB}} > 0$. The factor $\Delta N_{\text{XHB}}/\Delta N_{\text{HB}} < 0$, and increasing the enthalpic bonus J_H reduces the transition pressure P_t between the unfolded and the native states. This effect is the same regardless of protein size because the behavior of $\Delta N_{\text{XHB}}/\Delta N_{\text{HB}}$ is independent of chain length; ΔN_{XHB} and ΔN_{HB} are both size-dependent quantities, but both scale in the same way with chain length. The changes in these quantities are directly connected to the differences between the structures of the native and unfolded states. Ideally, the native state structure is maximally compact and the denatured state structure is fully extended, regardless of protein size, so that the ratio $\Delta N_{\text{XHB}}/\Delta N_{\text{HB}}$ in that case is constant.

The effect of the entropic cost on cold denaturation can be determined from the slope of the cold-denaturation line given by Eq. 10, also derived in Appendix B,

$$\frac{dP}{dT} \Big|_t = \frac{\Delta S}{\Delta v \Delta N_{\text{HB}}}, \quad (10)$$

where ΔS is the change in total system entropy upon unfolding. Since, as already noted, the transition to the unfolded state involves $\Delta N_{\text{HB}} < 0$, and noting that $\Delta v > 0$, then $dP/dT_t > 0$ when $\Delta S < 0$ and $dP/dT_t < 0$ if $\Delta S > 0$. At low temperatures the enthalpic bonus of interfacial hydrogen bonding dominates, driving the formation of an extended structure (Fig. 3 c) with the maximum number of interfacial hydrogen bonds formed. This cold-denatured state has a lower degeneracy than the native state (Fig. 3 a) and the protein transition upon cold unfolding has an inherent negative contribution to ΔS . It is an artifact of the model that the cold-denatured state is not an ensemble of disordered protein conformations since these are too high in energy to be stable at low temperatures (unlike for thermal denaturation at higher temperatures). Because the cold-denatured state has a larger number of interfacial hydrogen bonds than the native state, the water has a negative contribution to ΔS as long as there is an entropic penalty ($\lambda_b > \lambda_h$). Increasing the entropic penalty for interfacial hydrogen bonds increases the magnitude of the water contribution to the entropy decrease and thereby increases dP/dT_t , as seen in Fig. 4.

In contrast to cold unfolding, which is driven both by entropy and enthalpy effects, thermal denaturation at higher temperatures is an entropy-driven transition. The partial opening of the protein upon thermal denaturation breaks a few bulk hydrogen bonds ($\Delta N_{\text{HB}} < 0$), increasing both the protein and water disorder ($\Delta S > 0$). The simulations also show that the number of interfacial hydrogen bonds remains generally constant upon thermal denaturation ($\Delta N_{\text{XHB}} \approx 0$). The expression for the thermal denaturation temperature at zero pressure, derived in Appendix B, can be simplified to

$$T_t \Big|_{P_t=0} \approx -J \frac{\Delta N_{\text{HB}}}{\Delta S}. \quad (11)$$

Fig. 6 shows the effect of protein size on the thermal denaturation temperature. As the number of protein monomers

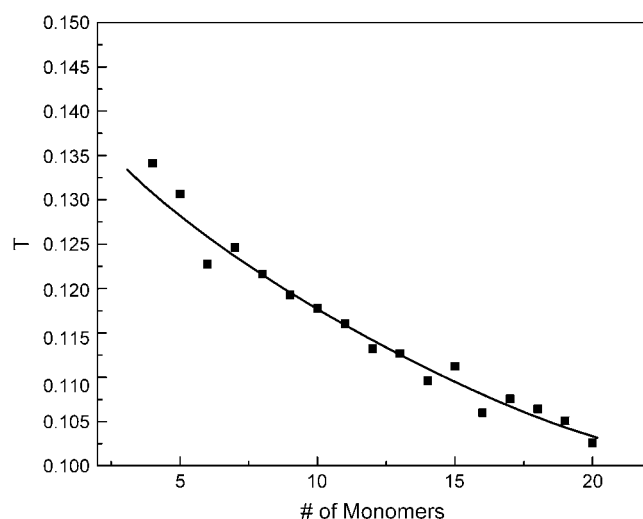


FIGURE 6 Thermal denaturation temperature at zero pressure for proteins of various sizes. $J_H/J = 0.2$, $\Delta v/v_0 = 0.348$, $\lambda_h = 0$, $\lambda_b = 1$, and $q = 30$ were used for all proteins. The line is a guide to the eye. Irregularities in the trend of decreasing thermal denaturation temperature with protein size are due to the discrete nature of the lattice. Equation 11 connects the structure of the native and denatured states to the thermal denaturation temperature through the change in entropy upon unfolding. The degeneracy of the native, compact state does not increase regularly with protein size. For example, a 9-mer or 16-mer has a square-shaped native state, while other protein sizes have rougher surfaces.

increases, the protein native state becomes less stable at high temperature. The destabilization is caused by the increasing gap between the entropies of the folded and denatured states. For each additional monomer added to the protein, the folded state's entropy will increase only slightly, associated with the increasing degeneracy of the compact protein configurations. However, the unfolded states' entropy will increase faster with protein size because of the larger number of disordered but mostly compact protein configurations common in the thermal-denatured state. ΔN_{HB} does not change with protein size because only one or two hydrogen bonds must break to allow the protein to transition from the compact folded state to mostly compact states. The net effect is that ΔS increases as the number of monomers increases, reducing T_d . This general trend is also observed experimentally, as the thermal

denaturation of single-domain proteins shows a negative correlation with protein size (52).

Fig. 7 examines the entropy and volume changes upon unfolding in our model and in a phenomenological model based on experimental studies of the most typical proteins (1). While cold unfolding and high pressure thermal unfolding in our model show the same denaturation thermodynamics as experiments, it is clear that the model does not reproduce the typical phenomenological slope of the phase diagram for thermal denaturation at ambient (low) pressure. Experimentally, there typically is a point on the denaturation curve where the slope of the phase transition for thermal denaturation is nearly infinite, corresponding to a volume change upon unfolding $\Delta V \approx 0$. This point is lacking in our model, along with regions of positive volume change upon unfolding. The cause originates in the model, where Eq. 3 directly links the volume of the system to the number of hydrogen bonds. For our model, denaturation is always associated with a negative volume change because protein unfolding involves the breaking of hydrogen bonds. A discussion of the volumetric properties of small hydrophobic solutes based on our model and their relation to the volumetric behavior associated with protein folding is given in Appendix C. There it is shown that, for small solutes, the model also correctly mimics most of the trends with temperature and pressure seen experimentally. Nevertheless, our model does show a point on the denaturation curve where $\Delta S \approx 0$, allowing for a distinct separation between cold denaturation ($\Delta S < 0$) and thermal denaturation ($\Delta S > 0$).

To relate the model results to experimental protein phase diagrams, we converted the temperature and pressure into dimensional quantities. A value of 23 kJ/mol was used in the temperature scaling for the average strength of a hydrogen bond, J . To scale the pressure we used 18 cm³/mol for the molar volume of water. The value of $\Delta v/v_0$ was chosen to approximate experimental values of the volume expansion of a water molecule upon forming a hydrogen bond. Using the densities of ice and liquid water of 0.917 and 1 g/cm³ at 0°C, the molar volume change upon freezing is 1.63 cm³/mol of water. The ratio of the heat of fusion to the heat of sublimation indicates that $\sim 13\%$ of hydrogen bonds are broken upon ice melting. An individual water molecule in ice has two

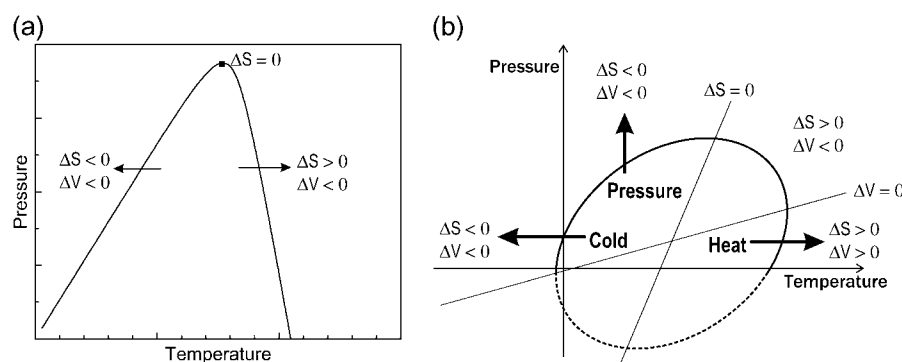


FIGURE 7 A comparison between the thermodynamics of unfolding in (a) our model and in (b) a schematic summary of experimental results. Panel b was adapted with permission from Hawley (1).

hydrogen bonds per molecule, therefore, on average, 0.26 hydrogen bonds per molecule are broken upon melting. Dividing the molar volume change upon freezing ($1.63 \text{ cm}^3/\text{mol}$) by the fraction of hydrogen bonds per molecule formed upon freezing (0.26) gives an estimate for the volume change upon forming a mole of hydrogen bonds, or $\Delta v = 6.27 \text{ cm}^3/\text{mol}$.

For a parameter selection of $J_H/J = 0.4$, $\lambda_h = 0$, $\lambda_b = 5$, $q = 110$, and $\Delta v/v_0 = 0.348$, the phase diagram of a model 20-mer is shown in Fig. 8. Pressure denaturation of the model protein is in the kbar region, of the same order of magnitude as the experimental results shown in Fig. 1. The temperatures for thermal and cold denaturation at ambient pressure are between 20 and 40°C below those seen experimentally. The model underestimates these temperatures because of the lack of favorable internal protein-protein interactions such as hydrogen-bonding and electrostatics. Including these forces might confer additional thermal stability to the protein.

Finally, a comparison between our model predictions and those of water-implicit protein models yields an interesting observation. The thermal denaturation of proteins in the original HP model is a broad transition, occurring over a range of dimensionless temperatures of $\mathcal{O}(1)$ (32). Our model clearly exhibits a much sharper transition between the native and denatured states, as shown in Fig. 2. The explicit inclusion of water gives rise to sharper phase transitions, in agreement with experimental observations. It remains to be seen whether sharp transitions are an artifact of the homopolymer case, or if heteropolymers would also exhibit this phenomenon.

CONCLUSIONS

We have developed a model for an all-hydrophobic homopolymer in water based on the thermodynamics of the

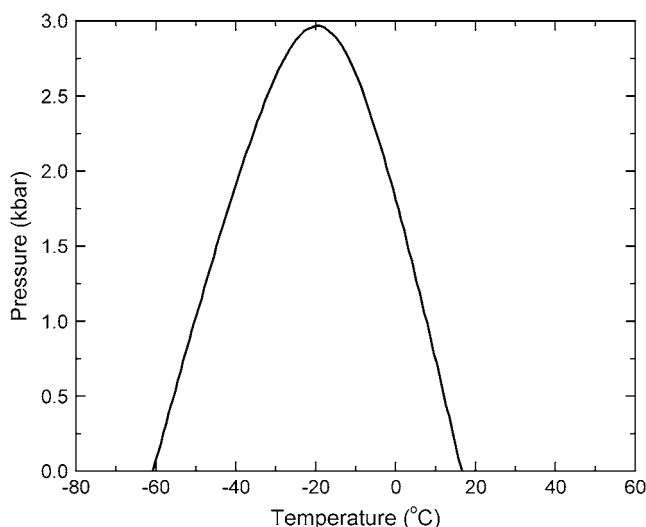


FIGURE 8 Contour of 50% folded probability for a model 20-mer with temperature and pressure converted into dimensional quantities using $J = 23 \text{ kJ/mol}$ and $v_0 = 18 \text{ cm}^3/\text{mol}$. Parameter values are $J_H/J = 0.4$ and $\lambda_b = 5$, $\lambda_h = 0$, $q = 110$, and $\Delta v/v_0 = 0.348$.

solvation of hydrophobic solutes. The model protein denatures at high temperature, low temperature, and high pressure, showing many of the same denaturation characteristics observed in experiments. Our model shows sharp unfolding transitions compared to water-implicit protein models. The key new feature here is the introduction of additional restrictions on the orientation for hydrogen bonding at the protein interface compared to the bulk. The two-tiered set of hydrogen-bonding interactions for the water modulates the cold denaturation transition by balancing between the stability of the native and cold-denatured states.

Using a homopolymer to describe the protein limits our study to the effects of protein size and of the water-protein interaction. The model also shows a decrease in the protein configurational degrees of freedom upon cold unfolding, an unphysical feature that we plan to improve upon. Calculations are in progress on a heteropolymer model, with both hydrophobic and polar monomers, as in the HP model (32). Incorporating details of the chemistry of proteins into the model will allow us to investigate how sequence selection and composition can affect the range of native state stability. We also plan to investigate three-dimensional systems, as well as the impact of correlation among the orientations of hydrogen bonds on each water molecule.

APPENDIX A: BIASED PROTEIN TRIAL MOVES

In addition to simple one-monomer and two-monomer translation trial moves, we used biased protein monomer translation moves to improve the sampling of rare protein configurations. In these biased trial moves, one or two monomers of the protein are translated without disrupting the hydrogen bonding structure of the solvent around it. To keep the number of hydrogen bonds constant, we bias the selection of water orientations for the water molecule which translates into the site formerly occupied by the protein monomer. This type of bias allows the protein to effectively explore configurations when the solvent is highly structured. To balance the improved sampling of biased trial moves with the shorter computation time of unbiased trial moves, 50% of protein translation trial moves are unbiased and 50% are biased.

The transition matrix that determines the probability to perform a one-monomer trial move from o to n is

$$T(o \rightarrow n) = p_i(o \rightarrow n)p_j(o \rightarrow n)p_w(o \rightarrow n)p_\sigma(o \rightarrow n), \quad (12)$$

where p_i is the probability of selecting monomer at site i for translation, p_j is the probability of selecting site j for the monomer to translate into, p_w is the probability of translating water w at site j back to site i , and p_σ is the probability of giving water molecule w the set of bonding arm orientations $\{\sigma\}$ ($\{\sigma\} = \{\sigma_{i1}, \sigma_{i2}, \sigma_{i3}, \sigma_{i4}\}$). In the biased trial move, all of these probabilities are symmetric, except p_σ , as we bias the selection of these orientations to keep the number of hydrogen bonds formed by water w (N_{HB}) constant from state o to state n .

Water w has a total of four hydrogen-bonding arms that are faced with several options in the new site depending on their neighbors. If a bonding arm points toward the protein it can have one of q orientations since the water molecule cannot hydrogen-bond with the protein. If a bonding arm points toward other water molecules the arms can either hydrogen-bond by matching their orientation to their neighbor or form nonbonding pairs. The total number of bonding arm pairs irrespective of their bonding status is denoted by N_{pairs} . To maintain a constant value of N_{HB} for water w , N_{HB} of the N_{pairs} bonding arm pairs are selected at random to be hydrogen-bonded

and the orientations set accordingly. The remaining $N_{\text{pairs}} - N_{\text{HB}}$ nonbonding pairs are given nonbonding orientations at random. If $N_{\text{HB}} > N_{\text{pairs}}$, the move is rejected automatically.

Based on these criteria, the probability of selecting orientations for water w is given by

$$p_{\sigma}(o \rightarrow n) = \left(\frac{1}{\binom{N_{\text{pairs}}}{N_{\text{HB}}}} \right) \prod_{i=1}^{N_{\text{HB}}} \left(\frac{1}{2\lambda_h + 1} \right) \times \prod_{i=N_{\text{HB}}}^{N_{\text{pairs}}} \left(\frac{1}{q - (2\lambda_h + 1)} \right) \prod_{i=N_{\text{pairs}}}^4 \left(\frac{1}{q} \right). \quad (13)$$

The first term is the probability of selecting a set of N_{HB} bonding pairs out of the N_{pairs} total bonding arms for hydrogen-bonding. The second term is the probability of selecting appropriate hydrogen-bonding orientations for those N_{HB} bonding arms. The third term is the probability of selecting appropriate nonbonding orientations for the remaining pairs. The final term is the probability of selecting any orientation for the bonding arms facing protein monomers.

Detailed balance requires that the opposing fluxes between states o and n be statistically equal, satisfying the relation

$$p(o)T(o \rightarrow n)A(o \rightarrow n) = p(n)T(n \rightarrow o)A(n \rightarrow o), \quad (14)$$

where p is the equilibrium probability of a state and A is the acceptance probability of a transition. Since the equilibrium probability of a state is the inverse of its density of states, we can derive the acceptance criteria:

$$\frac{A(o \rightarrow n)}{A(n \rightarrow o)} = \frac{\Omega(o) N_{\text{pairs}}(n)! (N_{\text{pairs}}(o) - N_{\text{HB}})!}{\Omega(n) N_{\text{pairs}}(o)! (N_{\text{pairs}}(n) - N_{\text{HB}})!} \times \left(\frac{q - (2\lambda_h + 1)}{q} \right)^{N_{\text{pairs}}(n) - N_{\text{pairs}}(o)}. \quad (15)$$

The principle is the same for a biased two-monomer trial move, with some additions. With two translating water molecules there are now eight bonding arms that are given biased orientations. Moreover, the translating waters can be subject to either bulk or interfacial hydrogen bonding criteria. The probability for selecting a set of orientations is

$$p_{\sigma}(o \rightarrow n) = \left(\frac{1}{\binom{N_{\text{pairs}}}{N_{\text{HB}}}} \right) \prod_{k=1}^{N_{\text{HB},i}} \left(\frac{1}{2\lambda_h + 1} \right) \prod_{k=N_{\text{HB},i}}^{N_{\text{pairs},i}} \left(\frac{1}{q - (2\lambda_h + 1)} \right) \times \prod_{k=1}^{N_{\text{HB},b}} \left(\frac{1}{2\lambda_b + 1} \right) \times \prod_{k=N_{\text{HB},b}}^{N_{\text{pairs},b}} \left(\frac{1}{q - (2\lambda_b + 1)} \right) \prod_{k=N_{\text{pairs}}}^8 \left(\frac{1}{q} \right), \quad (16)$$

where the subscripts i and b denote interfacial and bulk, respectively. The acceptance criteria for a biased two-monomer move is

$$\frac{A(o \rightarrow n)}{A(n \rightarrow o)} = \frac{\Omega(o) N_{\text{pairs}}(n)! (N_{\text{pairs}}(o) - N_{\text{HB}})!}{\Omega(n) N_{\text{pairs}}(o)! (N_{\text{pairs}}(n) - N_{\text{HB}})!} \left(\frac{2\lambda_h + 1}{q - (2\lambda_h + 1)} \right)^{\Delta N_{\text{HB},i}} \times (q - (2\lambda_h + 1))^{\Delta N_{\text{pairs},i}} \times \left(\frac{2\lambda_b + 1}{q - (2\lambda_b + 1)} \right)^{\Delta N_{\text{HB},b}} (q - (2\lambda_b + 1))^{\Delta N_{\text{pairs},b}} q^{-\Delta N_{\text{pairs}}}, \quad (17)$$

where the change in a quantity such as ΔN_{pairs} is $N_{\text{pairs}}(n) - N_{\text{pairs}}(o)$.

APPENDIX B: ANALYTICAL APPROXIMATION FOR TWO-STATE TRANSITIONS

The probability of any state, i , specified by N_{HB} and N_{XHB} can be calculated from simulation data for any pressure and temperature by

$$p_i(P, T) = \frac{\Omega_i \exp(-(U_i + PV_i)/k_B T)}{\Delta(P, T)}, \quad (18)$$

where Δ is the isothermal-isobaric partition function and k_B is Boltzmann's constant; Ω_i is the degeneracy of state i , while U_i and V_i are the energy and volume of state i , calculated from Eqs. 2 and 3. At a two-state transition between states 1 and 2, $p_1 = p_2$. Equating p_1 and p_2 and taking the natural logarithm gives the relationship

$$\ln \Omega_1 - (U_1 + P_1 V_1)/k_B T_1 = \ln \Omega_2 - (U_2 + P_1 V_2)/k_B T_1 \quad (19)$$

where P_1 and T_1 are the transition pressure and temperature. Using Boltzmann's relation $S_i = k_B \ln \Omega_i$ to replace the density of states with the entropy of state i and multiplying by k_B reduces the equation to

$$S_1 - (U_1 + P_1 V_1)/T_1 = S_2 - (U_2 + P_1 V_2)/T_1. \quad (20)$$

Substituting for the energy and volume using Eqs. 2 and 3 and rearranging yields the relation

$$T_1 \Delta S = -J \Delta N_{\text{HB}} - J_H \Delta N_{\text{XHB}} + P_1 \Delta v \Delta N_{\text{HB}}. \quad (21)$$

ΔN_{HB} , ΔN_{XHB} , and ΔS denote the difference in the respective property between states 1 and 2. Recall that Δv is not the change in a property between states 1 and 2, but instead the model parameter describing the uniform expansion of the lattice upon hydrogen-bond formation.

Equation 21 explicitly links the system states specified by N_{HB} and N_{XHB} , the model parameters J , J_H , and Δv , and the macroscopic variables T_1 and P_1 . An adaptation of the Clapeyron equation for this model can be derived by solving for P_1 in Eq. 21 and taking the derivative with respect to temperature:

$$\left. \frac{dP}{dT} \right|_t = \frac{\Delta S}{\Delta v \Delta N_{\text{HB}}}. \quad (22)$$

Equations 21 and 22 allow us to examine the shape of the protein phase diagram in greater detail and to investigate more deeply which mechanisms contribute to cold-, pressure-, and heat-denaturation. Two limiting cases are used to study the effects of model parameters on the thermodynamics. We derive the pressure at which a transition occurs between two ground states by solving for P_1 in Eq. 21 when $T_1 = 0$:

$$P_1 \Big|_{T_1=0} = \frac{J}{\Delta v} + \frac{J_H}{\Delta v} \frac{\Delta N_{\text{XHB}}}{\Delta N_{\text{HB}}}. \quad (23)$$

This expression gives the transition pressure between two ground states: the cold-denatured state stable at high pressures and the native state stable at low pressures.

We can also use the transition temperature at zero pressure to study thermal denaturation:

$$T_t \Big|_{P_t=0} = -J \frac{\Delta N_{HB}}{\Delta S} - J_H \frac{\Delta N_{XHB}}{\Delta S}. \quad (24)$$

This analysis is an approximation valid for a two-state transition without significantly populated intermediate states. The simulation results presented in this article show that this approximation is essentially exact during cold denaturation at low temperatures because both the native and cold-denatured states are well-defined and are the only highly populated states. Because thermal denaturation involves a transition into an ensemble of denatured states, the analysis is a less exact description at higher temperatures.

APPENDIX C: PARTIAL MOLAR VOLUME CALCULATIONS

As noted by Kauzmann (9) and mentioned in the Introduction, the volume change of transfer of hydrophobic solutes into water and the volume change of protein unfolding typically exhibit different dependences on pressure. Simulations of small hydrophobic solutes in water were performed to probe the model's ability to describe volumetric properties and to determine if the discrepancies pointed out by Kauzmann are observed. The solutes examined were smaller versions of the model homopolymer: one-site, two-site, and flexible three-site hydrophobic solutes in a fully occupied lattice of water. Changing the solute concentration by replacing water molecules with solute molecules on the lattice induces changes in the system volume at any given temperature and pressure. From the slope of this trend, we can calculate the quantity $(\partial V / \partial N_1)_{T,P,N}$, where N_1 is the number of solute molecules, N_2 is the number of solvent molecules, and the N subscript denotes a fixed number of occupied lattice sites. Note that this quantity is not the partial molar

volume of the solute, but a relationship between the two can be derived by examining the total differential for the volume,

$$dV = \left(\frac{\partial V}{\partial T} \right)_{P,N_1,N_2} dT + \left(\frac{\partial V}{\partial P} \right)_{T,N_1,N_2} dP + \left(\frac{\partial V}{\partial N_1} \right)_{T,P,N_2} dN_1 + \left(\frac{\partial V}{\partial N_2} \right)_{T,P,N_1} dN_2, \quad (25)$$

where the solute and solvent partial molar volumes (\bar{v}_1 and \bar{v}_2 , respectively) appear as

$$\left(\frac{\partial V}{\partial N_1} \right)_{T,P,N_2} = \bar{v}_1, \quad \left(\frac{\partial V}{\partial N_2} \right)_{T,P,N_1} = \bar{v}_2. \quad (26)$$

The solute's partial molar volume can be related to the quantity estimated from simulation results by taking the partial derivative of Eq. 25 with respect to N_1 while fixing the temperature, pressure, and total number of lattice sites, which yields the relation

$$\left(\frac{\partial V}{\partial N_1} \right)_{T,P,N} = \bar{v}_1 + \bar{v}_2 \left(\frac{\partial N_2}{\partial N_1} \right)_{T,P,N}. \quad (27)$$

The quantity $(\partial N_2 / \partial N_1)_{T,P,N}$ is -1 for a one-site solute, -2 for a two-site solute, and so forth. At infinite dilution Eq. 27 reduces to

$$\left(\frac{\partial V}{\partial N_1} \right)_{T,P,N} = \bar{v}_1^\infty - v_2, \quad (28)$$

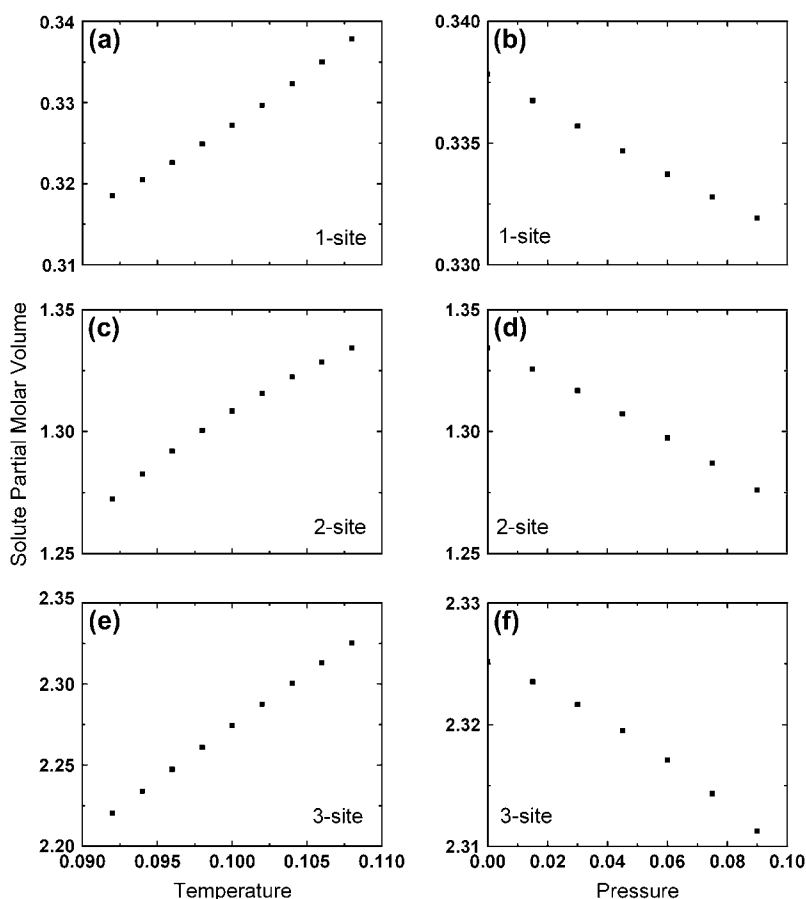


FIGURE 9 Partial molar volumes of the model hydrophobic solutes in water, in units of v_0 . Data from graphs *a*, *c*, and *e* are at constant $P = 0$. Data from graphs *b*, *d*, and *f* are at constant $T = 0.108$. Parameter values are $J_H/J = 0.2$, $\lambda_b = 3$, $\lambda_h = 0$, $q = 70$, and $\Delta v/v_0 = 0.348$.

for the case of a one-site solute, where \bar{v}_1^∞ is the partial molar volume of the solute at infinite dilution. v_2 is the molar volume of the solvent, which we can calculate from pure water simulations.

The temperature and pressure behavior of the partial molar volume of our model solutes in water correspond qualitatively to experimental trends for small apolar solutes. Fig. 9, *a*, *c*, and *e*, show that the partial molar volumes of each of the model solutes increases with increasing temperature. This trend matches the experimental observations of Masterton, who observed increasing partial molar volumes with increasing temperature for methane, ethane, propane, and benzene (53). The calculations also show that partial molar volumes decrease with increasing pressure (Fig. 9, *b*, *d*, and *f*), conforming to the trends observed experimentally for methane (54), benzene, and toluene (55).

As stated in the Introduction, the measured volume change upon transfer from a hydrophobic phase into water typically, although not always, exhibits a different pressure dependence than the volume change upon protein unfolding. The volume change upon hydrophobic transfer for a model solute can be estimated as the difference between the partial molar volume of the solute in water and the molar volume of the pure solute,

$$\Delta v_{\text{transfer}} = \bar{v}_1 - v_1. \quad (29)$$

The model definition for the molar volume of the pure solute is $N_{\text{sites}}v_0$, where N_{sites} is simply the number of sites comprising the solute (i.e.: 1, 2, or 3 in our case). In units of v_0 , it reduces simply to the number of monomers in the solute, i.e., 1 for a one-site solute, 2 for a two-site solute, etc. We note that v_0 is a temperature- and pressure-independent parameter, and hence our model for a hydrophobic homopolymer in water is not designed to predict the thermodynamic properties of a pure hydrophobic species.

Given this definition, we observe negative values of $\Delta v_{\text{transfer}}$ for each solute over the ranges of temperature and pressure shown in Fig. 9. The partial molar volume of the solutes under these conditions remains less than the molar volume of the pure solute. This behavior at low pressures matches the observed experimental transfer volume changes, where the transfer of methane from liquid hexane into water at 1 bar corresponds to a molar volume decrease of 22.7 cm³/mol (5). However, at high pressures where small hydrophobic solute transfer volumes are positive (9), this model predicts negative transfer volumes.

The behavior of $\Delta v_{\text{transfer}}$ for model solutes is consistent with the volume change upon unfolding for the model protein. As shown schematically in Fig. 7 *a*, the model protein exhibits a volume decrease upon unfolding at low and high pressures. While this does not conform to Kauzmann's assertions about the pressure dependence of protein volume changes (9), nor to experimental observations of many proteins such as chymotrypsinogen (1), some proteins such as staphylococcal nuclease (3) show a volume decrease upon thermal denaturation at low pressures. The factors that determine whether a protein has a positive or negative volume change upon unfolding are still a matter of some debate (56). The model protein presented here captures the correct volumetric properties of a subset of real proteins.

We thank Pradeep Kumar and H. Eugene Stanley for helpful discussions. We also acknowledge the Texas Advanced Computing Center at the University of Texas at Austin for high performance computing resources.

P.G.D. and P.J.R. gratefully acknowledge the support of the National Science Foundation (Collaborative Research in Chemistry grants No. CHE0404699 (P.G.D.) and No. CHE0404695 (P.J.R.)); the U.S. Department of Energy, Division of Chemical Sciences, Geosciences, and Biosciences, Office of Basic Energy Sciences, grant No. DE-FG02-87ER13714 (P.G.D.); and the R.A. Welch Foundation (grant No. F0019 to P.J.R.).

REFERENCES

- Hawley, S. A. 1971. Reversible pressure-temperature denaturation of chymotrypsinogen. *Biochemistry*. 10:2436–2442.
- Heremans, K., and L. Smeller. 1998. Protein structure and dynamics at high pressure. *Biochim. Biophys. Acta*. 1386:353–370.
- Ravindra, R., and R. Winter. 2003. On the temperature-pressure free-energy landscape of proteins. *ChemPhysChem*. 4:359–365.
- Dill, K. A. 1990. Dominant forces in protein folding. *Biochemistry*. 29: 7133–7155.
- Kauzmann, W. 1959. Some factors in the interpretation of protein denaturation. *Adv. Protein Chem.* 14:1–63.
- Rose, G. D., A. R. Geselowitz, G. J. Lesser, R. H. Lee, and M. H. Zehfus. 1985. Hydrophobicity of amino-acid residues in globular-proteins. *Science*. 229:834–838.
- Singer, S. J. 1962. The properties of proteins in nonaqueous solvents. *Adv. Protein Chem.* 17:1–68.
- Baldwin, R. L. 1986. Temperature-dependence of the hydrophobic interaction in protein folding. *Proc. Natl. Acad. Sci. USA*. 83:8069–8072.
- Kauzmann, W. 1987. Protein stabilization—thermodynamics of unfolding. *Nature*. 325:763–764.
- Hummer, G., S. Garde, A. E. Garcia, M. E. Paulaitis, and L. R. Pratt. 1998. The pressure dependence of hydrophobic interactions is consistent with the observed pressure denaturation of proteins. *Proc. Natl. Acad. Sci. USA*. 95:1552–1555.
- Hummer, G., S. Garde, A. E. Garcia, M. E. Paulaitis, and L. R. Pratt. 1998. Hydrophobic effects on a molecular scale. *J. Phys. Chem. B*. 102: 10469–10482.
- Lum, K., D. Chandler, and J. D. Weeks. 1999. Hydrophobicity at small and large length scales. *J. Phys. Chem. B*. 103:4570–4577.
- ten Wolde, P. R. 2002. Hydrophobic interactions: an overview. *J. Phys. Cond. Matt.* 14:9445–9460.
- ten Wolde, P. R., and D. Chandler. 2002. Drying-induced hydrophobic polymer collapse. *Proc. Natl. Acad. Sci. USA*. 99:6539–6543.
- Athawale, M. V., G. Goel, T. Ghosh, T. M. Truskett, and S. Garde. 2007. Effects of lengthscales and attractions on the collapse of hydrophobic polymers in water. *Proc. Natl. Acad. Sci. USA*. 104: 733–738.
- Duan, Y., and P. A. Kollman. 1998. Pathways to a protein folding intermediate observed in a 1-microsecond simulation in aqueous solution. *Science*. 282:740–744.
- De Mori, G. M. S., C. Micheletti, and G. Colombo. 2004. All-atom folding simulations of the villin headpiece from stochastically selected coarse-grained structures. *J. Phys. Chem. B*. 108:12267–12270.
- Wu, X. W., and B. R. Brooks. 2004. beta-hairpin folding mechanism of a nine-residue peptide revealed from molecular dynamics simulations in explicit water. *Biophys. J.* 86:1946–1958.
- Rhee, Y. M., E. J. Sorin, G. Jayachandran, E. Lindahl, and V. S. Pande. 2004. Simulations of the role of water in the protein-folding mechanism. *Proc. Natl. Acad. Sci. USA*. 101:6456–6461.
- Zhou, R. H., X. H. Huang, C. J. Margulis, and B. J. Berne. 2004. Hydrophobic collapse in multidomain protein folding. *Science*. 305: 1605–1609.
- Sanjeev, B. S., and S. Vishveshwara. 2004. Protein-water interactions in ribonuclease A and angiogenin: a molecular dynamics study. *Proteins*. 55:915–923.
- Paliwal, A., D. Asthagiri, D. P. Bossev, and M. E. Paulaitis. 2004. Pressure denaturation of staphylococcal nuclease studied by neutron small-angle scattering and molecular simulation. *Biophys. J.* 87:3479–3492.
- Shen, M. Y., and K. F. Freed. 2002. All-atom fast protein folding simulations: the villin headpiece. *Proteins*. 49:439–445.
- Cui, B. X., M. Y. Shen, and K. F. Freed. 2003. Folding and misfolding of the papillomavirus E6 interacting peptide E6ap. *Proc. Natl. Acad. Sci. USA*. 100:7087–7092.
- Chowdhury, S., M. C. Lee, and Y. Duan. 2004. Characterizing the rate-limiting step of Trp-cage folding by all-atom molecular dynamics simulations. *J. Phys. Chem. B*. 108:13855–13865.
- Irbach, A., and S. Mohanty. 2005. Folding thermodynamics of peptides. *Biophys. J.* 88:1560–1569.

27. Rousseau, R., E. Schreiner, A. Kohlmeier, and D. Marx. 2004. Temperature-dependent conformational transitions and hydrogen-bond dynamics of the elastin-like octapeptide GVG(VPGVG): a molecular-dynamics study. *Biophys. J.* 86:1393–1407.
28. Herges, T., and W. Wenzel. 2005. In silico folding of a three helix protein and characterization of its free-energy landscape in an all-atom force field. *Phys. Rev. Lett.* 94:018101.
29. Herges, T., and W. Wenzel. 2004. An all-atom force field for tertiary structure prediction of helical proteins. *Biophys. J.* 87:3100–3109.
30. Paschek, D., S. Gnanakaran, and A. E. Garcia. 2005. Simulations of the pressure and temperature unfolding of an alpha-helical peptide. *Proc. Natl. Acad. Sci. USA.* 102:6765–6770.
31. Paschek, D., and A. E. Garcia. 2004. Reversible temperature and pressure denaturation of a protein fragment: A replica exchange molecular dynamics simulation study. *Phys. Rev. Lett.* 93:238105.
32. Lau, K. F., and K. A. Dill. 1989. A lattice statistical-mechanics model of the conformational and sequence-spaces of proteins. *Macromolecules.* 22:3986–3997.
33. Chan, H. S., and K. A. Dill. 1991. Sequence space soup of proteins and copolymers. *J. Chem. Phys.* 95:3775–3787.
34. De Los Rios, P., and G. Caldarelli. 2000. Putting proteins back into water. *Phys. Rev. E.* 62:8449–8452.
35. Caldarelli, G., and P. De Los Rios. 2001. Cold and warm denaturation of proteins. *J. Biol. Phys.* 27:229–241.
36. Salvi, G., S. Molbert, and P. De Los Rios. 2002. Design of lattice proteins with explicit solvent. *Phys. Rev. E.* 66:061911.
37. Salvi, G., and P. De Los Rios. 2003. Effective interactions cannot replace solvent effects in a lattice model of proteins. *Phys. Rev. Lett.* 91:258102.
38. Muller, N. 1990. Search for a realistic view of hydrophobic effects. *Accounts Chem. Res.* 23:23–28.
39. Lee, B., and G. Graziano. 1996. A two-state model of hydrophobic hydration that produces compensating enthalpy and entropy changes. *J. Am. Chem. Soc.* 118:5163–5168.
40. Dill, K. A. 1985. Theory for the folding and stability of globular-proteins. *Biochemistry.* 24:1501–1509.
41. Dill, K. A., D. O. V. Alonso, and K. Hutchinson. 1989. Thermal stabilities of globular-proteins. *Biochemistry.* 28:5439–5449.
42. Cheung, J. K., P. Shah, and T. M. Truskett. 2006. Heteropolymer collapse theory for protein folding in the pressure-temperature plane. *Biophys. J.* 91:2427–2435.
43. Marques, M. I., J. M. Borreguero, H. E. Stanley, and N. V. Dokholyan. 2003. Possible mechanism for cold denaturation of proteins at high pressure. *Phys. Rev. Lett.* 91:138103.
44. Lassalle, M. W., H. Yamada, and K. Akasaka. 2000. The pressure-temperature free energy-landscape of staphylococcal nuclease monitored by H-1 NMR. *J. Mol. Biol.* 298:293–302.
45. Frank, H. S., and M. W. Evans. 1945. Free volume and entropy in condensed systems. 3. Entropy in binary liquid mixtures—partial molal entropy in dilute solutions—structure and thermodynamics in aqueous electrolytes. *J. Chem. Phys.* 13:507–532.
46. Sastry, S., P. G. Debenedetti, F. Sciortino, and H. E. Stanley. 1996. Singularity-free interpretation of the thermodynamics of supercooled water. *Phys. Rev. E.* 53:6144–6154.
47. Rebelo, L. P. N., P. G. Debenedetti, and S. Sastry. 1998. Singularity-free interpretation of the thermodynamics of supercooled water. II. Thermal and volumetric behavior. *J. Chem. Phys.* 109:626–633.
48. Franzese, G., M. I. Marques, and H. E. Stanley. 2003. Intramolecular coupling as a mechanism for a liquid-liquid phase transition. *Phys. Rev. E.* 67:011103.
49. Silverstein, K. A. T., A. D. J. Haymet, and K. A. Dill. 1999. Molecular model of hydrophobic solvation. *J. Chem. Phys.* 111:8000–8009.
50. Rossky, P. J., and D. A. Zichi. 1982. Molecular librations and solvent orientational correlations in hydrophobic phenomena. *Faraday Symp. Chem. Soc.* 17:69–78.
51. Wang, F. G., and D. P. Landau. 2001. Determining the density of states for classical statistical models: A random walk algorithm to produce a flat histogram. *Phys. Rev. E.* 64:056101.
52. Kumar, S., C. J. Tsai, and R. Nussinov. 2003. Temperature range of thermodynamic stability for the native state of reversible two-state proteins. *Biochemistry.* 42:4864–4873.
53. Masterton, W. L. 1954. Partial molal volumes of hydrocarbons in water solution. *J. Chem. Phys.* 22:1830–1833.
54. Hnedkovsky, L., R. H. Wood, and V. Majer. 1996. Volumes of aqueous solutions of CH₄, CO₂, H₂S, and NH₃ at temperatures from 298.15 K to 705 K and pressures to 35 MPa. *J. Chem. Therm.* 28: 125–142.
55. Sawamura, S., K. Kitamura, and Y. Taniguchi. 1989. Effect of pressure on the solubilities of benzene and alkylbenzenes in water. *J. Phys. Chem.* 93:4931–4935.
56. Meersman, F., L. Smeller, and K. Heremans. 2005. Extending the pressure-temperature state diagram of myoglobin. *Helv. Chim. Acta.* 88: 546–556.